ACS Catalysis

pubs.acs.org/acscatalysis Research Article

Assessing the Catalytic Role of Native Glucagon Amyloid Fibrils

Ashim Nandi,[⊥] Aoxuan Zhang,[⊥] Elad Arad, Raz Jelinek, and Arieh Warshel*

Cite This: *ACS Catal.* 2024, 14, 4656–4664 **Read Online**

ACCESS | Metrics & More | Article Recommendations | Supporting Information

ABSTRACT: Glucagon stands out as a pivotal peptide hormone, instrumental in controlling blood glucose levels and lipid metabolism. While the formation of glucagon amyloid fibrils has been documented, their biological functions remain enigmatic. Recently, we demonstrated experimentally that glucagon amyloid fibrils can act as catalysts in several biological reactions including esterolysis, lipid hydrolysis, and dephosphorylation. Herein, we present a multiscale quantum mechanics/molecular mechanics (QM/MM) simulation of the acylation step in the esterolysis of *para*-nitrophenyl acetate (*p*-NPA), catalyzed by native glucagon amyloid fibrils, serving as a model system to elucidate their catalytic function. This step entails a concerted mechanism, involving proton transfer from serine to histidine, followed by the nucleophilic attack of the serine oxy anion on the carbonyl carbon of *p*-NPA. We computed the binding energy and free-energy profiles of this reaction using the protein−dipole Langevin−dipole (PDLD) within the linear response approximation (LRA) framework (PDLD/S-LRA-2000) and the empirical valence bond (EVB) methods. This included simulations of the reaction in an aqueous environment and in the fibril, enabling us to estimate the catalytic effect of the fibril. Our EVB calculations obtained a barrier of 23.4 kcal mol^{-1} for the enzyme-catalyzed reaction compared to the experimental value of 21.9 kcal mol^{-1} (and a calculated catalytic effect of 3.2 kcal mol^{-1} compared to the observed effect of 4.7 kcal mol^{-1}). This close agreement together with the barrier reduction when transitioning from the reference solution reaction to the amyloid fibril provides supporting evidence to the catalytic role of glucagon amyloid fibrils. Moreover, employing the PDLD/S-LRA-2000 approach further reinforced exclusively the enzyme's catalytic role. The results presented in this study contribute significantly to our understanding of the catalytic role of glucagon amyloid fibrils, marking, to the best of our knowledge, the first-principles mechanistic investigation of fibrils using QM/MM methods. Therefore, our findings offer fruitful insights for future research into the mechanisms of related amyloid catalysis.

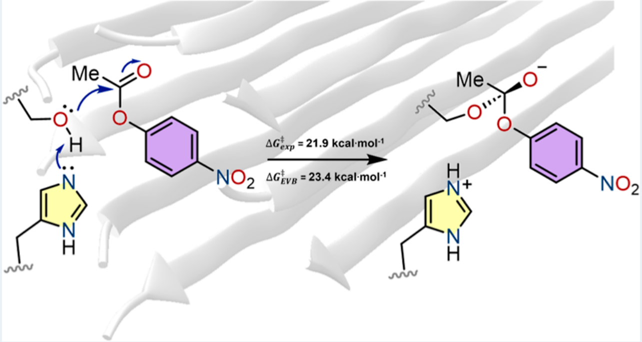

KEYWORDS: *amyloid fibrils, catalysis, kinetics, peptides and proteins, mechanisms, binding energy*

1. INTRODUCTION

Amyloids, initially identified as anomalous sugar deposits in various tissues, including diseased brains, were subsequently revealed to be protein-based structures.[1] Its specific structural characteristics were long shrouded in mystery until early X-ray diffraction studies on aggregated globulins provided hints of a distinctive design having intermolecular beta sheets oriented perpendicularly to the strand direction, forming the characteristic cross-β pattern seen in most amyloid structures.[1−3] While amyloids have often been linked to various human diseases such as Alzheimer's and Parkinson's,[4,5] it has become apparent that not only disease-related proteins adopt this structure. Surprisingly, many proteins can transition into the amyloid state under certain conditions, occasionally leading to new health-related issues.[6−9] Recent advances have further expanded our understanding, revealing that numerous human proteins, even those unrelated to pathological conditions, can adopt a fibrillar amyloid-like organization, both in laboratory settings (*in vitro*) and within living organisms (*in vivo*).[10−13]

Among these proteins is glucagon, a peptide hormone composed of 29 amino acid residues in conjunction with insulin that helps regulate blood glucose levels.[14,15] This hormone is present in a wide variety of animals and is primarily synthesized in the pancreas, specifically by α cells.[16,17] It holds a significant role in various metabolic pathways, influencing lipid metabolism, energy regulation, and amino acid metabolism.[15,18,19] Irregularities in glucagon levels can contribute to various pathological conditions, including insulin resistance (linked to type-2 diabetes) and glucagonoma, which involves an elevated turnover of amino acids in the liver and irregular triglyceride breakdown.[20−22]

Received: January 20, 2024
Revised: March 1, 2024
Accepted: March 4, 2024
Published: March 13, 2024

https://doi.org/10.1021/acscatal.4c00452

Though the exact biological functions of these glucagon fibrils have largely remained unexplored, it was suggested that amyloid fibrils as a group played a role in primitive catalytic reactions.[23,24] This phenomenon was first demonstrated in synthetic amyloid-like systems.[25,26] Our recent experimental work has unveiled the catalytic potential of amyloid fibers formed by peptides like Alzheimer's disease peptide amyloid-β (Aβ)[27] and glucagon,[28] particularly when they take on a fibrillar form, unlike their monomeric counterparts. This finding suggests that the polymeric structure of amyloid fibers offers unique catalytic sites on their surface.[29] Additionally, another independent research team has established that amyloid fibers formed by α-synuclein also exhibit enzyme-like catalytic properties in biological reactions.[30] Collectively, these findings have indicated that naturally occurring amyloids can catalyze a range of physiological and pathological reactions, distinguishing them from synthetic, predesigned amyloidogenic peptides. Given this emerging understanding, it encouraged us to delve into an atomistic examination of the catalytic mechanisms at play within glucagon amyloid fibrils using QM/MM approaches.

Estimation of the structure−function activity of amyloids originating from natural sequences is a challenging task: unlike other highly ordered proteinaceous systems, the amyloid state is a misfolded state.[4] Moreover, polymorphism is a key feature of amyloid fibrillar structures due to their assembly process and surrounding conditions.[31−33] Glucagon, in particular, was shown to form several polymorphs depending on the local microenvironment at the early stages of the protofibril assembly,[10,34] reflecting that the fibrils do not reach a singular global energy minimum.[35,36] However, all polymorphs consist of common features such as β-sheet assembly in which the strands are spread and oriented in juxtaposition with each other in an antiparallel fashion.[34] In respect to polymorphism, although it may slightly differ at the mature fibrillar level, the cross-β fashion remains dominant.

In the realm of enzyme catalysis, the hallmark is the accelerated pace of enzymatic reactions compared with their counterparts in reference aqueous solutions. To comprehensively assess the catalytic influence of the enzyme environment, it is essential to consider the corresponding reaction in a reference solution. The empirical valence bond (EVB) approach,[37−39] as outlined in Section 2.2, stands as a favored computational method in enzymology. Its appeal lies in its computational efficiency and its ability to seamlessly incorporate parameters relevant to the reference reaction.

This paper aims to shed light on the catalytic mechanism governing the esterolysis of *para*-nitrophenol acetate (*p*-NPA) by human glucagon fibrils,[28] using it as an illustrative model of catalysis, with a specific focus on the acylation step involving proton transfer and nucleophilic attack (PT-NA). Our investigation employs the protein−dipole Langevin−dipole (PDLD) within the linear response approximation (LRA) framework (PDLD/S-LRA-2000) method,[40] detailed in Section 2.1, for extensive binding energy calculations and qualitative assessments of catalytic activity in the studied system. We employed the EVB method for the rigorous elucidation of the reaction mechanism. For calibration of the EVB treatment, it is imperative to evaluate the thermodynamic and kinetic parameters of the reference reaction.[41] In this study, we derived the EVB parameters of the reference reaction in water through a combination of experimental and ab initio data, as previously reported in our works.[41] By combining these computational approaches, our work offers a deeper understanding of the catalytic mechanisms at play within glucagon amyloid fibrils.

2. COMPUTATIONAL METHODS

The catalytic effects were studied by using the EVB method. The corresponding activation free energies were calculated by the free energy perturbation/umbrella sampling (FEP/US).[42] The EVB and FEP/US approaches, previously detailed and utilized in numerous prior studies,[37,38] are concisely reviewed in the Supporting Information and, partially, below. Additionally, for a thorough examination of the binding energy calculations and a qualitative evaluation of the catalytic effect, we also employed the PDLD/S-LRA-2000 method, which is succinctly described in the following sections.

The structure of the studied enzyme was sourced from the Protein Data Bank, specifically utilizing the NMR structure found under PDB entry 6NZN.[13] The substrate employed in the present study was *p*-NPA, which was optimized using the M06-2X/Def2-TZVP level of theory in the Gaussian16 software suite.[43] Following this, the optimized structure was docked into the enzyme using AutoDock software.[44] A variety of docked structures were evaluated, as discussed below. The atomic charges of the QM region were determined from electrostatic potential (ESP)[45] charges computed by Gaussian16 at the M06-2X/Def2-TZVP level with the inclusion of the SMD solvation model.[46] These resultant charges were utilized to generate the restrained electrostatic potential (RESP)-fitted charges[47] via AmberTools.[48] The RESP charges were exclusively applied to the substrate and the reacting residues, serine and histidine, whereas the ENZYMIX force field[49] was utilized for the atoms of the enzyme and water. All the calculations were carried out using the MOLARIS-XG package.[49]

2.1. EVB Method.

The reliability of the EVB method hinges on conducting enzyme calculations relative to the same reaction taking place in a water environment, as mentioned earlier. The energetics of the reference reaction in water is based on a combination of experimental information and ab initio data, which was detailed in our previous work[41] and is depicted in Figure S1. To create the reference system, we employed a surface constraint all-atom solvent (SCAAS)[50] sphere with a radius of 20 Å to solvate the system. This surface-constrained water sphere was encompassed by a 10 Å surface layer composed of Langevin dipoles,[51,52] followed by the bulk solvent. Long-range electrostatic effects were treated using the local reaction field (LRF) method.[53] The system underwent relaxation in seven sequential steps, commencing at a temperature of 5 K. Subsequently, the temperature was gradually increased to the experimental temperature of 310 K over an overall relaxation time of 200 ps, resulting in the generation of five distinct starting structures. For the reference system, mirroring the reacting system in water, we adhered to the same protocol as that employed in the enzyme calculations. The determination of reaction free energy profiles was carried out using the EVB method, wherein, in the case of two resonance states, the ground-state energy (E_g) was computed through the solution of the secular equation given by

$$\begin{vmatrix} H_{11} - E_g & H_{12} \\ H_{21} & H_{22} - E_g \end{vmatrix}$$

Here, H_{11} and H_{12} represent the diabatic energies of the reactant and product states, respectively. Throughout the simulation, the reaction progresses using a free energy perturbation (FEP) technique, which alters the system's potential (V) by transitioning from the reactant state to the product state through a coupling parameter (λ) given by

$$V(\lambda) = \lambda \cdot H_{11} + (1 - \lambda) \cdot H_{22} \tag{1}$$

The collected data were subsequently employed in a specialized umbrella sampling approach[54] to construct the actual free energy profile of the reaction.

In this study, each simulation was conducted on five different replicas. Each replica underwent an FEP simulation consisting of 31 frames, where the coupling parameter λ was incrementally changed in 31 equal steps of 0.03. Each MD frame involved a 20 ps equilibration under the potential $V(\lambda)$. The five replicas began with distinct initial configurations obtained through five successive 20 ps equilibration steps. For the reference reaction in water, the serine and histidine residues were Cα-methylated. During the MD simulations, a force of 10 kcal/mol/Å^2 was applied to keep the Cα atoms in their original positions. Otherwise, the FEP protocol in water mirrored that in the enzyme.

The EVB simulations for the reference solution reaction were calibrated by adjusting the gas phase shift and the off-diagonal coupling to match the reaction profile presented in Figure S1. After the EVB parameters were calibrated, they remained unchanged for simulating the reaction in the enzyme. In these simulations, the full atomistic effects of the entire enzyme were considered, except for atoms outside the solvation sphere, which were constrained by 10 kcal/mol/Å^2 to their original positions. Consequently, due to these constraints, some degrees of freedom contributing to the reaction entropy were not considered. The EVB parameters, including the RESP charges, are provided in the Supporting Information.

2.2. Semimacroscopic PDLD/S Method. Besides utilizing the EVB method, the enzyme's catalytic effect can also be estimated using a modified semimacroscopic version of the PDLD method within the LRA framework, termed PDLD/S-LRA-2000.[40,55,56] This approach similar to our original PDLD/S-LRA method involves scaling the nonelectrostatic term (C) (see below). In this method, the protein is considered a medium with a "dielectric constant" ($\varepsilon_{\mathrm{im}}$), signifying all implicitly treated contributions and involving thermodynamic cycles by adjusting the solvent's (water) dielectric constant (ε_{w}) from its actual value ε_{w} to $\varepsilon_{\mathrm{im}}$. Within the LRA framework,[57] the PDLD/S free energies accommodate the effect of protein and solvent reorganization throughout the binding cycle, as detailed in our previous works.[57,58] In our current work, the binding free energy is expressed as

$$\Delta G_{\mathrm{bind}}^{\mathrm{PDLD/S\text{-}LRA\text{-}2000}} \cong \alpha \Delta G_{\mathrm{bind}}^{\mathrm{elec}} + Cx\Delta G_{\mathrm{bind}}^{\mathrm{non\text{-}elec}}$$
$$\cong \frac{1}{2}[(\langle U_{\mathrm{elec,l}}^{\mathrm{p}}\rangle_{Q=Q_0} + \langle U_{\mathrm{elec,l}}^{\mathrm{p}}\rangle_{Q=0}) - (\langle U_{\mathrm{elec,l}}^{\mathrm{w}}\rangle_{Q=Q_0} + \langle U_{\mathrm{elec,l}}^{\mathrm{w}}\rangle_{Q=0})] + Cx\Delta G_{\mathrm{bind}}^{\mathrm{non-elec}} \tag{2}$$

where the superscripts "p" and "w" refer to protein and water environments, respectively. "Q" represents the substrate atoms' charge distribution, which alternates between its actual charge distribution and zero throughout the binding cycle (see refs 40 and 55). The $< >_{\mathrm{Q}}$ notation indicates an average over configurations from MD simulations with the specified Q. The nonelectrostatic term accounts for binding free energy from hydrophobic effects, van der Waals, water penetration, and entropy contribution.

The scaling factor C for the nonelectrostatic contribution, critical in our analysis, was treated with care following our 2000 benchmark study.[56] This C factor is not a universal constant but is specific to the studied system, influenced by a complex balance of thermodynamic contributions like van der Waals interactions, hydrophobic effects, water penetration, and configurational entropy changes, further explained in ref 56. For the current study, we determined an optimal C value of 0.70, which effectively calibrates the calculated binding affinity with experimental observation (*vide infra*).

The electrostatic contributions are obtained from the effective PDLD/S-LRA potentials

$$\bar{U}_{\mathrm{elec,l}}^{\mathrm{p}} = \left[(\Delta G_{\mathrm{sol}}^{\mathrm{l+p}} - \Delta G_{\mathrm{sol}}^{\mathrm{l'+p}})\left(\frac{1}{\varepsilon_{\mathrm{in}}} - \frac{1}{\varepsilon_{\mathrm{w}}}\right) + \Delta G_{\mathrm{sol}}^{\mathrm{l}}\left(1 - \frac{1}{\varepsilon_{\mathrm{w}}}\right) + \frac{U_{q\mu}^{\mathrm{l}}}{\varepsilon_{\mathrm{in}}} + \frac{U_{\mathrm{intra}}^{\mathrm{l}}}{\varepsilon_{\mathrm{in}}} \right]_{\mathrm{B}} \tag{3}$$

$$\bar{U}_{\mathrm{elec,l}}^{\mathrm{w}} = \left[\Delta G_{\mathrm{sol}}^{\mathrm{l}}\left(1 - \frac{1}{\varepsilon_{\mathrm{w}}}\right) + \frac{U_{\mathrm{intra}}^{\mathrm{l}}}{\varepsilon_{\mathrm{in}}} \right]_{\mathrm{UB}} \tag{4}$$

In the above expressions, the solvation free energy, $\Delta G_{\mathrm{sol}}^{\mathrm{solute}}$, of a system is assessed by the microscopic (unscaled) PDLD method. The superscripts of the solvation energy, "l + p" and "l′ + p", refer to ligand−protein complexes in their charged states and the same complex with a nonpolar ligand (i.e., all atomic charges of the ligand are assigned to zero). The parameter, not directly tied to the actual protein "dielectric constant", accounts for implicitly treated contributions.[48,49] Typically, when protein reorganization energy is explicitly considered, it is reasonable to use it.[49,50] The $U_{q\mu}^{\mathrm{l}}$ value reflects the vacuum interaction between ligand charges and protein dipoles. The $U_{\mathrm{intra}}^{\mathrm{l}}$ value is the intramolecular electrostatic interaction of the ligand. The subscripts "B" and "UB" refer to the sampling of the configurations in protein (bound, B) and in water (unbound, UB), respectively. Also, nonelectrostatic contributions are estimated by

$$\Delta G_{\mathrm{bind}}^{\mathrm{non\text{-}elec}} = \Delta G_{\mathrm{bind}}^{\mathrm{hyd}} + \Delta G_{\mathrm{bind}}^{\mathrm{vdw}} \tag{5}$$

where $\Delta G_{\mathrm{bind}}^{\mathrm{hyd}}$ represents a field-dependent hydrophobic term, estimating the relevant surface area considering the local field on each Langevin dipole in the initial "solvation shell". $\Delta G_{\mathrm{bind}}^{\mathrm{vdw}}$ pertains to the van der Waals contribution.

Finally, calculating the catalytic effect entails assessing the binding energy in both the ground and transition states by employing

$$(\Delta\Delta g^{\ddagger})^{\mathrm{w}\to\mathrm{p}} = (\Delta G_{\mathrm{bind}}^{\ddagger} - \Delta G_{\mathrm{bind}}^{\circ})^{\mathrm{w}\to\mathrm{p}} \tag{6}$$

where $\Delta G_{\mathrm{bind}}^{\ddagger}$ and $\Delta G_{\mathrm{bind}}^{\circ}$ represent the binding energy of the transition and ground states, respectively. The mean of eq 2 for both states is derived by using a central force field, wherein the minimum energy structure aligns with that of the correspond-

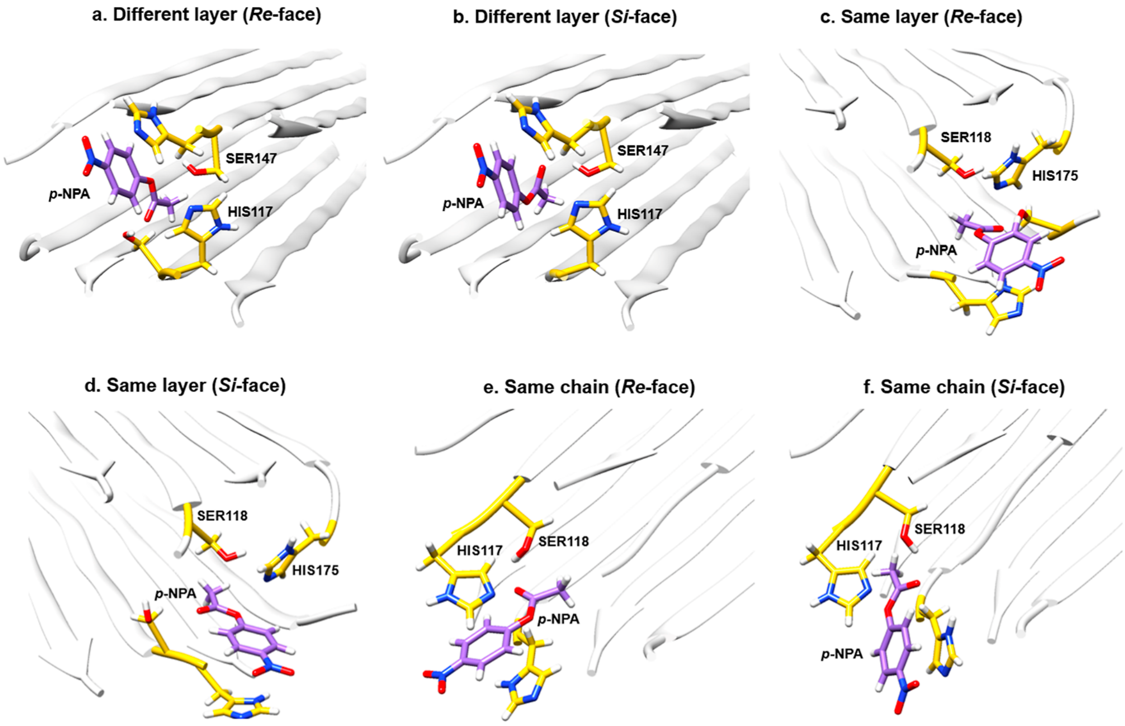

Figure 1. Docked structures showcasing various poses of the substrate *p*-NPA: (a) positioned on the different layer with the carbonyl carbon facing the *Re*-side of the NA attack, (b) located on the different layer with the carbonyl carbon facing the *Si*-side, (c) on the same layer with the carbonyl carbon oriented toward the *Re*-side, (d) on the same layer with the carbonyl carbon facing the *Si*-side, (e) on the same chain with the carbonyl carbon facing the *Re*-side, and (f) on the same chain with the carbonyl carbon oriented toward the *Si*-side. Note: the residue numbering in the hundreds is attributed to the presence of 10 conformers in the PDB NMR structures. The structures shown here are selected for their relevance in kinetic and binding studies.

ing EVB surface. The relevant charges from the central force field are adapted from the corresponding EVB charges.

The substrate-binding free energy was calculated by the PDLD method in its LRA (PDLD/S-LRA) using a sampling of 4 different configurations collected at every 10 ps of successive MD relaxation. In these calculations, we used a dielectric constant of 4, whose effect accounts for the poor configurational sampling and lack of nuclear and electronic polarization effects.[59,60]

To ensure the reproducibility of our results, we have included both our docked structures, parameters, and complete input files in the Supporting Information. Additionally, a GitHub link to access these materials is provided therein.

3. RESULTS AND DISCUSSION

A comparative scrutiny of various glucagon variants in our prior experimental study facilitated the localization of the catalytic activity to an enzyme-like pocket formed on the surface of the glucagon fibril, which includes the histidyl-serine domain at the peptide's N-terminus. Based on this knowledge, we carried out extensive docking and binding energy calculations of the different poses of the substrate *p*-NPA bound around this catalytic dyad. This was followed by investigating into the catalytic mechanism using the EVB and PDLD/S-LRA-2000 methods.

3.1. Binding Energy. The binding mode of *p*-NPA within the fibril has not yet been determined experimentally. To address this, we utilized an NMR-determined structure (PDB entry: 6NZN) with ten submitted conformers as a template to search for potential binding modes. Since the catalytic residues are exclusively located at the peptide termini, as mentioned above, we conducted an automatic docking targeting the termini of the fibril across all ten conformers. These docked structures were then manually adjusted to produce suitable starting points for subsequent binding and reaction energy profile calculations. Notably, we explored several configurations of our substrate and binding poses during the docking process, namely, the *Re* and *Si* faces of the carbonyl carbon of *p*-NPA binding on the outer surface, same chain, same layer, and different layer on the amyloid fibril (see Figure 1). To further validate our findings, we employed the PDLD/S-LRA-2000 method to determine the binding energy for each docking mode. For each mode, we conducted five distinct simulations, each initialized with different structures sampled by the ENZYMIX force field. The results presented are the averages from these simulations. During every PDLD/S-LRA simulation, the LRA calculation was executed on ten different configurations sampled throughout the trajectory.

The binding energies for the various poses are listed in Table 1. It is evident that the binding energies across different configurations are relatively similar, with notable exceptions being the surface (not depicted in Figure 1), different layer (*Re*), and same layer (*Re*) poses. These values are in close alignment with the experimentally observed binding energy. This suggests the possibility of multiple binding sites. However, it also highlights the challenge of identifying the optimal binding pose due to the extremely flat surface of the fibril and the lack of distinct catalytic pockets. Nevertheless, the binding energies are in excellent agreement with the observed value of −3.34 kcal mol^{-1}, particularly for the poses with the different layer (*Si*), the same chain (*Re*), and the same layer (*Si*), which have binding energies of −3.23, −3.40, and

Table 1. PDLD/S-LRA-2000 Binding Energy Calculations for Different Poses[a]

poses	ΔG_{calc} (kcal mol^{-1})
surface	−1.29
different layer (*Re*)	−1.34
different layer (*Si*)	−3.23
same layer (*Re*)	−1.39
same layer (*Si*)	−3.42
same chain (*Re*)	−3.40
same chain (*Si*)	−2.82

[a] From the experimental K_m measured at pH 7.4, we approximated the binding energy using the equation $\Delta G_{\text{exp}} = -RT \ln K_m = -3.34$ kcal mol^{-1}.

−3.42 kcal mol^{-1}, respectively (refer to Figure 1b,e,f). For the downstream EVB free energy calculations, the same chain (*Re*) pose was selected due to the proper orientations of the catalytic residues, Ser118 and His117, facilitating the PT-NA process (see Figure 1e). This is in contrast to other potential poses, where the proton of Ser147 is oriented away from the N_δ of His117 (Figure 1b). It is worth noting that we also investigated the reaction mechanism with the same layer (*Si*) pose but found its free energy profile to be kinetically unfavorable with an EVB activation barrier of over 25 kcal mol^{-1}.

3.2. EVB Reaction Mechanism. Our study centers on the acylation step, which involves a concerted PT-NA process, as illustrated in Scheme 1. The calibration of the reference solution was performed using our previously determined free energy profile for the acylation step of esterolysis, as mentioned above. It is important to note that the reference solution reaction in our prior study was executed via a stepwise reaction involving PT, followed by NA. While for the current study we computed the EVB free energy profile for this stepwise mechanism, the intermediate formed post-PT was found to have an ascending free energy curve lacking minima, suggesting a fleeting intermediate formation. Consequently, we shifted our attention to exploring the concerted PT-NA, hypothesizing it as a possible mechanism and identifying it as the rate-determining state (RDS). To calibrate the reference solution for the concerted PT-NA, we derived the activation and reaction energy from the overall free energy profile of the stepwise mechanism, based on our previous study.[41] This study assumed that the RDS remained consistent across both mechanisms. The reference profile can be found in the Supporting Information.

The EVB reaction profiles for the reference reaction in water and in the glucagon fibril enzyme are shown in Figure 2. The energetics for the concerted PT-NA reference reaction in water was obtained using a distance constraint of 10 kcal/mol/Å^2 at 3.5 Å between the O and N_δ atoms of Ser118 and His117 for the PT and between the O of Ser118 and the carbonyl carbon atom of the ester group for the NA. In contrast, within the fibril, we applied a 2 kcal/mol/Å^2 distance constraint for the same atom pairs.

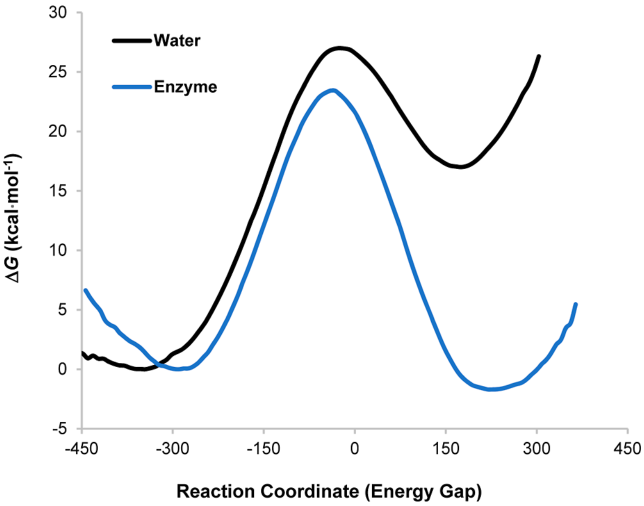

Figure 2. Free energy profiles for the concerted PT-NA (acylation step) in the esterolysis of *p*-NPA. The reference profile in solution is represented in black, while the amyloid fibril-catalyzed profile is illustrated in blue. The reaction coordinate is defined by the energy difference between EVB states 2 and 1, a measure typically used to display EVB free-energy profiles (derivation in the Supporting Information).

The computed EVB free energy barrier for the PT-NA (acylation step) reaction is 23.4 kcal mol^{-1}, aligning closely with the experimental value of 21.9 kcal mol^{-1}. The reaction

Scheme 1. Docked Structure of the Substrate *p*-NPA in the NMR-Determined Structure of the Glucagon Amyloid Fibril (PDB Entry: 6NZN)[13] (Left) and the Schematic Reaction Showing Concerted PT-NA (Acylation Step) in the Esterolysis of *p*-NPA (Right)[a]

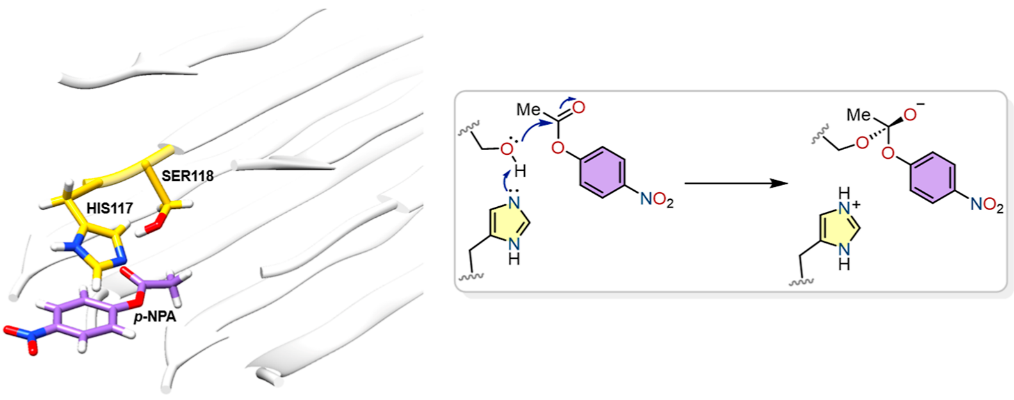

[a] In the EVB representation, the reactant is described by state 1 and the product by state 2.

free energy for the enzyme-catalyzed reaction is exergonic, registering at −1.7 kcal mol^{-1}. Both the experimental and calculated kinetic parameters for the enzyme-catalyzed reaction are listed in Table 2.

Table 2. Experimental and Calculated Kinetic Parameters, Alongside Calculated Reaction Free Energy for the Glucagon Fibril-Catalyzed Esterolysis of *p*-NPA[a]

k_{exp}^{cat} (s^{-1})	$\Delta G_{exp}^{\ddagger}$ (kcal mol^{-1})	$\Delta G_{calc}^{\ddagger}$ (kcal mol^{-1})	ΔG_{calc} (kcal mol^{-1})
2.5×10^{-3}	21.9	23.4	−1.7

[a] Experimental free energy barrier $\Delta G_{exp}^{\ddagger}$ was derived from the experimental rate constant, k_{exp}^{cat}, measured at pH 7.4, utilizing the Eyring−Polanyi equation.

In a water environment, the reaction barrier for the acylation step, as determined from experimental and ab initio calculations in our previous study (and used in the current study for calibration), was found to be 26.6 kcal mol^{-1}. The reaction free energy in water is 16.9 kcal mol^{-1}. Notably, this value is destabilized by 18.6 kcal mol^{-1} compared to that for the glucagon fibril active site, suggesting that the charged intermediates following the PT-NA are highly stabilized and the reaction becomes exothermic within the enzyme, whereas it is highly endothermic in the water environment. A comparison of the activation free energies between the reference solution and enzymatic environments reveals that the glucagon fibril lowers the barrier by 3.2 kcal mol^{-1} relative to that of water. By employing the transition-state theory, the corresponding increase in the reaction rate constant can thus be estimated to be about 2 orders of magnitude ($k_{calc}^{cat} \sim 2 \times 10^{-4}$ s^{-1}) at the experimental temperature. This implies that the reaction in the enzymatic environment proceeds much faster compared to the reaction in the aqueous solution, which is extremely slow ($k_{calc}^{wat} \sim 1.1 \times 10^{-6}$ s^{-1}) under a normal experimental setup. This strongly provides atomistic evidence of the catalytic effect of the glucagon fibril in the esterolysis of *p*-NPA, in agreement with our previous experimental study.

3.3. PDLD/S-LRA-2000 Calculations. To further validate our findings, we also assessed the activation energy using the PDLD/S-LRA-2000 method, as outlined in Section 2.2. The binding energies for the ground and transition states were determined by employing the substrate and a pertinent fragment of the catalytic dyad (illustrated in Scheme 1), with charges derived from the charge set of the diabetic state 1. The binding energy calculations involved generating relaxed structures through MD simulations, conducted under the conditions summarized in Table 3. Although this study was not as extensive as the EVB study, its primary aim was to evaluate the electrostatic energies in configurations proximal to the NMR structure. Our calculations indicate a reduction in $\Delta\Delta g^{\ddagger}$ when transitioning from a water to an enzyme environment, yielding a value of −3.9 kcal mol^{-1} (refer to Table 3). This very closely replicates the EVB activation barrier and further substantiates the evidence of the catalytic contribution of the glucagon fibril.

Table 3. PDLD/S-LRA-2000 Activation Energy for the Acylation Step[a]

ΔG_{bind}° (kcal mol^{-1})	$\Delta G_{bind}^{\ddagger}$(kcal mol^{-1})	$(\Delta\Delta g^{\ddagger})^{w\rightarrow p}$ (kcal mol^{-1})
−4.2	−8.2	−3.9

[a] The value of $(\Delta\Delta g^{\ddagger})^{(w\rightarrow p)}$ was derived from eq 6, evaluating the pertinent $\Delta G_{bind}^{\ddagger}$ and ΔG_{bind}° by averaging the corresponding $\Delta\Delta G_{bind}$ across 4 configurations. Each of these was taken after 20 ps of MD simulation using ε_p = 4 and the charge set of the diabetic state 1. Initial configurations were produced by conducting 20 ps simulations utilizing the reaction coordinates of the EVB surfaces of both the reactant state and the TS.

3.4. Origin of the Catalytic Effect of the Glucagon Fibril. The EVB/FEP and PDLD/S-LRA-2000 computational methods both systematically reflected the enzymatic effect of the glucagon fibril on the acylation step, aligning well with the experimental findings detailed above. This overall catalytic effect is linked to the stabilization of the TS. Upon examining the TS configuration closely, we observed that the benzene ring of *p*-NPA is engaged in a π-stacking interaction with His118 and His146 at both the TS and tetrahedral intermediate (TI) stages. More importantly, the carbonyl oxygen of *p*-NPA forms a hydrogen bond with Ser147 at a distance of 2.3 Å at the TS, while the oxyanion hole created in the TI is further stabilized by Ser147, positioned 2.0 Å away. Notably, the distance facilitating the NA between the oxygen of Ser117 and the carbonyl carbon of *p*-NPA is significantly shorter in the fibril compared to a reference water solution at the TS (2.59 Å vs 3.36 Å). These interactions become more dominant and persist during the formation of the TI in the enzyme (see Figure 3 for visual inspection), leading to further stabilization of the intermediate and thereby resulting in the exergonicity of the reaction. This underscores the idea that enzymes largely attribute their catalytic effect to preorganized electrostatics.[61] The dominant influence of electrostatics is evident in the reaction that we examined. In particular, the reaction leads to the formation of the oxyanion-Ser147 pair. As a result, the reaction profiles are affected by the environment. The preorganized electrostatics within the enzyme provide an additional barrier reduction, which might be vital in physiological contexts.

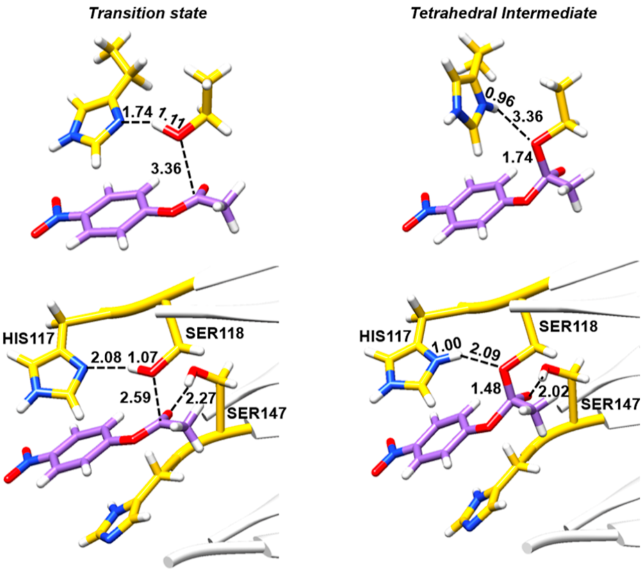

Figure 3. Illustration of the TS and tetrahedral intermediate structures within a reference water solution (top) and a native glucagon amyloid fibril environment (bottom), highlighting selected bond distances in Angstroms. The water sphere has been omitted for clarity.

4. CONCLUSIONS

In summary, our study involved a comprehensive exploration of the acylation step in the *p*-NPA esterolysis process catalyzed by glucagon amyloid fibrils. By employing the state-of-the-art EVB method and the PDLD/S-LRA-2000 approach, we unraveled the intricacies of this reaction mechanism, treating it as an instructive test for the catalytic capabilities of glucagon amyloid fibrils—a topic we had previously investigated through experimental means.

Our computational analysis yielded an EVB-free activation energy of 23.4 kcal mol^{-1}, a value consistent with the experimentally determined activation energy of 21.9 kcal mol^{-1}. This alignment serves as evidence affirming the validity of the proposed mechanism governing the amyloid fibril-catalyzed esterolysis of *p*-NPA. Furthermore, through a comparative assessment of activation free energies in enzymatic and water environments, we estimated the catalytic effect—the reduction in the activation barrier—imparted by glucagon amyloid fibrils to be approximately 3.2 and 3.9 kcal mol^{-1} by the EVB and PDLD/S-LRA-2000 methods, respectively. This finding furnishes atomistic proof, substantiating the catalytic role played by amyloid fibrils. The key contributor to this catalytic effect appears to be preorganized electrostatics, specifically the formation of the oxyanion-Ser147 pair during the concerted PT-NA process. Consequently, the reaction profiles exhibit a pronounced dependence on the surrounding environment. In the enzyme environment, the barrier is lowered, enabling the reaction from a thermodynamic standpoint, while the prearranged enzyme electrostatics make a supplementary and likely crucial contribution to barrier reduction for physiological relevance.

In summary, given that most studies on catalytic amyloids use the esterolysis of *p*-NPA as a benchmark reaction for measuring catalytic activity, our work offers deeper insight into the catalytic role of glucagon amyloid fibrils, offering valuable insights with broader implications for catalytic amyloid. We anticipate that this work will facilitate further exploration into the atomic-level mechanisms of related amyloid fibrils.

■ ASSOCIATED CONTENT

Supporting Information

The Supporting Information is available free of charge at https://pubs.acs.org/doi/10.1021/acscatal.4c00452.

Concise overview of the computational methods, free energy profile for the reference reaction, parameters employed, and link to a GitHub repository with all the input files and PDBs (PDF)

■ AUTHOR INFORMATION

Corresponding Author

Arieh Warshel – *Department of Chemistry, University of Southern California, Los Angeles, California 90089-1062, United States;* orcid.org/0000-0001-7971-5401; Email: warshel@usc.edu

Authors

Ashim Nandi – *Department of Chemistry, University of Southern California, Los Angeles, California 90089-1062, United States;* orcid.org/0000-0002-1090-7664

Aoxuan Zhang – *Department of Chemistry, University of Southern California, Los Angeles, California 90089-1062, United States*

Elad Arad – *Ilse Katz Institute (IKI) for Nanoscale Science and Technology, Ben-Gurion University of the Negev, Beer-Sheva 8410501, Israel; Department of Chemistry, Ben-Gurion University of the Negev, Beer-Sheva 8410501, Israel; Department of Chemical Engineering, Columbia University, New York, New York 10027, United States*

Raz Jelinek – *Ilse Katz Institute (IKI) for Nanoscale Science and Technology, Ben-Gurion University of the Negev, Beer-Sheva 8410501, Israel; Department of Chemistry, Ben-Gurion University of the Negev, Beer-Sheva 8410501, Israel;* orcid.org/0000-0002-0336-1384

Complete contact information is available at: https://pubs.acs.org/10.1021/acscatal.4c00452

Author Contributions

$^{\perp}$A.N., A.Z. are co-first authors.

Notes

The authors declare no competing financial interest.

■ ACKNOWLEDGMENTS

This work was supported by the National Institute of Health R35 GM122472 and the National Science Foundation Grant MCB 2142727.

■ REFERENCES

(1) Ke, P. C.; Zhou, R.; Serpell, L. C.; Riek, R.; Knowles, T. P. J.; Lashuel, H. A.; Gazit, E.; Hamley, I. W.; Davis, T. P.; Fändrich, M.; Otzen, D. E.; Chapman, M. R.; Dobson, C. M.; Eisenberg, D. S.; Mezzenga, R. Half a Century of Amyloids: Past, Present and Future. *Chem. Soc. Rev.* **2020**, *49* (15), 5473–5509.

(2) Riek, R. The Three-Dimensional Structures of Amyloids. *Cold Spring Harbor Perspect. Biol.* **2017**, *9* (2), a023572.

(3) Greenwald, J.; Riek, R. Biology of Amyloid: Structure, Function, and Regulation. *Structure* **2010**, *18* (10), 1244–1260.

(4) Chiti, F.; Dobson, C. M. Protein Misfolding, Amyloid Formation, and Human Disease: A Summary of Progress Over the Last Decade. *Annu. Rev. Biochem.* **2017**, *86* (1), 27–68.

(5) Alam, P.; Siddiqi, K.; Chturvedi, S. K.; Khan, R. H. Protein Aggregation: From Background to Inhibition Strategies. *Int. J. Biol. Macromol.* **2017**, *103*, 208–219.

(6) Sawaya, M. R.; Hughes, M. P.; Rodriguez, J. A.; Riek, R.; Eisenberg, D. S. The Expanding Amyloid Family: Structure, Stability, Function, and Pathogenesis. *Cell* **2021**, *184* (19), 4857–4873.

(7) Cao, Y.; Adamcik, J.; Diener, M.; Kumita, J. R.; Mezzenga, R. Different Folding States from the Same Protein Sequence Determine Reversible vs Irreversible Amyloid Fate. *J. Am. Chem. Soc.* **2021**, *143* (30), 11473–11481.

(8) Guijarro, J. I.; Sunde, M.; Jones, J. A.; Campbell, I. D.; Dobson, C. M. Amyloid Fibril Formation by an SH3 Domain. *Proc. Natl. Acad. Sci. U.S.A.* **1998**, *95* (8), 4224–4228.

(9) Buell, A. K. Stability Matters, Too - the Thermodynamics of Amyloid Fibril Formation. *Chem. Sci.* **2022**, *13* (35), 10177–10192.

(10) Pedersen, J. S. The Nature of Amyloid-like Glucagon Fibrils. *J. Diabetes Sci. Technol.* **2010**, *4*, 1357.

(11) Malishev, R.; Xu, W.; Pochan, D. J. The pro-apoptotic domain of BIM protein forms toxic amyloid fibrils. *Cell Mol Life Sci* **2021**, *78*, 2145.

(12) Jiménez, J. L.; Nettleton, E. J.; Liao, S.-Y. The protofilament structure of insulin amyloid fibrils. *Proc. Natl. Acad. Sci. U.S.A.* **2002**, *99*, 9196.

(13) Gelenter, M. D.; Smith, K. J.; Liao, S.-Y.; Mandala, V. S.; Dregni, A. J.; Lamm, M. S.; Tian, Y.; Xu, W.; Pochan, D. J.; Tucker, T. J.; Su, Y.; Hong, M. The peptide hormone glucagon forms amyloid fibrils with two coexisting *β*-strand conformations. *Nat. Struct. Mol. Biol.* **2019**, *26* (7), 592–598.

(14) Kawamori, D.; Kurpad, A. J.; Hu, J.; Liew, C. W.; Shih, J. L.; Ford, E. L.; Herrera, P. L.; Polonsky, K. S.; McGuinness, O. P.; Kulkarni, R. N. Insulin Signaling in α Cells Modulates Glucagon Secretion In Vivo. *Cell Metab.* **2009**, *9* (4), 350−361.

(15) Habegger, K. M.; Heppner, K. M.; Geary, N.; Bartness, T. J.; DiMarchi, R.; Tschöp, M. H. The Metabolic Actions of Glucagon Revisited. *Nat. Rev. Endocrinol.* **2010**, *6* (12), 689−697.

(16) Dunning, B. E.; Foley, J. E.; Ahrén, B. Alpha Cell Function in Health and Disease: Influence of Glucagon-like Peptide-1. *Diabetologia* **2005**, *48* (9), 1700−1713.

(17) Lefebvre, P. J. Glucagon and Adipose Tissue Lipolysis. In *Glucagon I*; Lefèbvre, P. J., Ed.; Springer: Berlin, Heidelberg, 1983; pp 419−440.

(18) Jens, J. H.; Albrechtsen, N. J. W. Glucagon and Amino Acids Are Linked in a Mutual Feedback Cycle: The Liver-α-Cell Axis. *Diabetes* **2017**, *66*, 235.

(19) Galsgaard, K. D.; Pedersen, J.; Knop, F. K.; Holst, J. J.; Wewer Albrechtsen, N. J. Glucagon Receptor Signaling and Lipid Metabolism. *Front. Physiol.* **2019**, *10*, 1−11.

(20) Holst, J. J.; Holland, W.; Gromada, J.; Lee, Y.; Unger, R. H.; Yan, H.; Sloop, K. W.; Kieffer, T. J.; Damond, N.; Herrera, P. L. Insulin and Glucagon: Partners for Life. *Endocrinology* **2017**, *158* (4), 696−701.

(21) Boden, G.; Tappy, L.; Jadali, F.; Hoeldtke, R. D.; Rezvani, I.; Owen, O. E. Role of Glucagon in Disposal of an Amino Acid Load. *Am. J. Physiol. Endocrinol. Metabol.* **1990**, *259* (2), E225−E232.

(22) Adeva-Andany, M. M.; Funcasta-Calderón, R.; Fernández-Fernández, C.; Castro-Quintela, E.; Carneiro-Freire, N. Metabolic Effects of Glucagon in Humans. *J. Clin. Transl. Endocrinol.* **2019**, *15*, 45−53.

(23) Friedmann, M. P.; Torbeev, V.; Zelenay, V.; Sobol, A.; Greenwald, J.; Riek, R. Towards Prebiotic Catalytic Amyloids Using High Throughput Screening. *PLoS One* **2015**, *10* (12), No. e0143948.

(24) Greenwald, J.; Riek, R. On the Possible Amyloid Origin of Protein Folds. *J. Mol. Biol.* **2012**, *421* (4−5), 417−426.

(25) Makhlynets, O. V.; Korendovych, I. V. Functional Frankensteins. *Nat. Chem.* **2016**, *8* (9), 823−824.

(26) Rufo, C.; Jelinek, R. Short peptides self-assemble to produce catalytic amyloids. *Nat. Chem.* **2014**, *6*, 303.

(27) Arad, E.; Baruch Leshem, A.; Rapaport, H.; Jelinek, R. β-Amyloid fibrils catalyze neurotransmitter degradation. *Chem Catal.* **2021**, *1* (4), 908−922.

(28) Arad, E.; Yosefi, G.; Kolusheva, S.; Bitton, R.; Rapaport, H.; Jelinek, R. Native Glucagon Amyloids Catalyze Key Metabolic Reactions. *ACS Nano* **2022**, *16* (8), 12889−12899.

(29) Arad, E.; Jelinek, R. Catalytic Amyloids. *Trends Chem.* **2022**, *4* (10), 907−917.

(30) Horvath, I.; Wittung-Stafshede, P. Amyloid Fibers of α-Synuclein Catalyze Chemical Reactions. *ACS Chem. Neurosci.* **2023**, *14* (4), 603−608.

(31) Close, W.; Neumann, M.; Schmidt, A.; Hora, M.; Annamalai, K.; Schmidt, M.; Reif, B.; Schmidt, V.; Grigorieff, N.; Fändrich, M. Physical Basis of Amyloid Fibril Polymorphism. *Nat. Commun.* **2018**, *9* (1), 699.

(32) Jesper, S. P.; Andersen, C. B.; Otzen, D. E. Amyloid structure - one but not the same: the many levels of fibrillar polymorphism. *The FEBS Journal* **2010**, *277*, 4591.

(33) Tycko, R. Amyloid Polymorphism: Structural Basis and Neurobiological Relevance. *Neuron* **2015**, *86*, 632.

(34) Andersen, C. B.; Hicks, M. R.; Vetri, V.; Vandahl, B.; Rahbek-Nielsen, H.; Thøgersen, H.; Thøgersen, I. B.; Enghild, J. J.; Serpell, L. C.; Rischel, C.; Otzen, D. E. Glucagon Fibril Polymorphism Reflects Differences in Protofilament Backbone Structure. *J. Mol. Biol.* **2010**, *397* (4), 932−946.

(35) Pedersen, J. S.; Dikov, D.; Flink, J. L.; Hjuler, H. A.; Christiansen, G.; Otzen, D. E. The Changing Face of Glucagon Fibrillation: Structural Polymorphism and Conformational Imprinting. *J. Mol. Biol.* **2006**, *355* (3), 501−523.

(36) Adamcik, J.; Mezzenga, R. Amyloid Polymorphism in the Protein Folding and Aggregation Energy Landscape. *Angew. Chem., Int. Ed.* **2018**, *57* (28), 8370−8382.

(37) Kamerlin, S. C. L.; Warshel, A. The EVB as a Quantitative Tool for Formulating Simulations and Analyzing Biological and Chemical Reactions. *Faraday Discuss.* **2010**, *145* (0), 71−106.

(38) Warshel, A.; Weiss, R. M. An empirical valence bond approach for comparing reactions in solutions and in enzymes. *J. Am. Chem. Soc.* **1980**, *102*, 6218−6226.

(39) Kamerlin, S. C. L. The empirical valence bond model: theory and applications. *Wiley Interdiscip. Rev. Comput. Mol. Sci.* **2011**, *1*, 30.

(40) Lee, F. S.; Chu, Z. T.; Warshel, A. Microscopic and Semimicroscopic Calculations of Electrostatic Energies in Proteins by the POLARIS and ENZYMIX Programs. *J. Comput. Chem.* **1993**, *14* (2), 161−185.

(41) Fuxreiter, M.; Warshel, A. Origin of the Catalytic Power of Acetylcholinesterase: Computer Simulation Studies. *J. Am. Chem. Soc.* **1998**, *120* (1), 183−194.

(42) Zwanzig, R. W. High-Temperature Equation of State by a Perturbation Method. I. Nonpolar Gases. *J. Chem. Phys.* **1954**, *22*, 1420.

(43) Frisch, M. J. *Gaussian 16*. Revision A03; Gaussian Inc: Wallingford CT, 2016.

(44) Morris, G. M.; Huey, R.; Lindstrom, W.; Sanner, M. F.; Belew, R. K.; Goodsell, D. S.; Olson, A. J. AutoDock4 and AutoDockTools4: Automated Docking with Selective Receptor Flexibility. *J. Comput. Chem.* **2009**, *30* (16), 2785−2791.

(45) Cox, S. R.; Williams, D. E. Representation of the molecular electrostatic potential by a net atomic charge model. *J. Comput. Chem.* **1981**, *2*, 304.

(46) Tomasi, J.; Mennucci, B.; Cammi, R. Quantum Mechanical Continuum Solvation Models. *Chem. Rev.* **2005**, *105*, 2999−3094.

(47) Bayly, C. I.; Cieplak, P.; Cornell, W.; Kollman, P. A. A Well-Behaved Electrostatic Potential Based Method Using Charge Restraints for Deriving Atomic Charges: The RESP Model. *J. Phys. Chem.* **1993**, *97* (40), 10269−10280.

(48) David, D. A.; Chu, Z. T.; Villa, J. The Amber biomolecular simulation programs. *J. Comput. Chem.* **2005**, *26*, 1668.

(49) Warshel, A.; Chu, Z. T.; Villa, J.; Strajbl, M.; Schutz, C.; Shurki, A.; Vicatos, S.; Plotnikov, N.; Schopf, P. *Molaris-Xg*. Version 9.15; University of Southern California: Los Angeles, 2012.

(50) Warshel, A.; King, G. Polarization Constraints in Molecular Dynamics Simulation of Aqueous Solutions: The Surface Constraint All Atom Solvent (SCAAS) Model. *Chem. Phys. Lett.* **1985**, *121* (1−2), 124−129.

(51) Warshel, A.; Levitt, M. Theoretical Studies of Enzymic Reactions: Dielectric, Electrostatic and Steric Stabilization of the Carbonium Ion in the Reaction of Lysozyme. *J. Mol. Biol.* **1976**, *103* (2), 227−249.

(52) Russell, S. T.; Warshel, A. Calculations of Electrostatic Energies in Proteins: The Energetics of Ionized Groups in Bovine Pancreatic Trypsin Inhibitor. *J. Mol. Biol.* **1985**, *185* (2), 389−404.

(53) Lee, F. S.; Warshel, A. A Local Reaction Field Method for Fast Evaluation of Long-range Electrostatic Interactions in Molecular Simulations. *J. Chem. Phys.* **1992**, *97* (5), 3100−3107.

(54) Hwang, J. K.; King, G.; Creighton, S. Simulation of free energy relationships and dynamics of SN2 reactions in aqueous solution. *J. Am. Chem. Soc.* **1988**, *110*, 5297.

(55) Singh, N.; Warshel, A. Absolute Binding Free Energy Calculations: On the Accuracy of Computational Scoring of Protein-Ligand Interactions. *Proteins: Struct., Funct., Bioinf.* **2010**, *78* (7), 1705−1723.

(56) Sham, Y. Y.; Chu, Z. T.; Tao, H.; Warshel, A. Examining methods for calculations of binding free energies: LRA, LIE, PDLD-LRA, and PDLD/S-LRA calculations of ligands binding to an HIV protease. *Proteins: Struct., Funct., Bioinf.* **2000**, *39* (4), 393−407.

(57) Lee, F. S.; Chu, Z.-T.; Bolger, M. B.; Warshel, A. Calculations of Antibody-Antigen Interactions: Microscopic and Semi-Microscopic

Evaluation of the Free Energies of Binding of Phosphorylcholine Analogs to McPC603. *Protein Eng. Des. Sel.* **1992**, *5* (3), 215−228.

(58) Muegge, I.; Tao, H.; Warshel, A. A Fast Estimate of Electrostatic Group Contributions to the Free Energy of Protein-Inhibitor Binding. *Protein Eng. Des. Sel.* **1997**, *10* (12), 1363−1372.

(59) Warshel, A.; Sharma, P. K.; Kato, M.; Parson, W. W. Modeling Electrostatic Effects in Proteins. *Biochim. Biophys. Acta, Proteins Proteomics* **2006**, *1764* (11), 1647−1676.

(60) Schutz, C. N.; Warshel, A. What Are the Dielectric "Constants" of Proteins and How to Validate Electrostatic Models? *Proteins: Struct., Funct., Bioinf.* **2001**, *44* (4), 400−417.

(61) Asadi, M.; Warshel, A. Analyzing the Reaction of Orotidine 5′-Phosphate Decarboxylase as a Way to Examine Some Key Catalytic Proposals. *J. Am. Chem. Soc.* **2023**, *145* (2), 1334−1341.